Available online at www.sciencedirect.com
SCIENCE DIRECT
Surface & Coatings Technology 200 (2006) 5767 – 5777
SURFACE & COATINGS TECHNOLOGY
www.elsevier.com/locate/surfcoat

Corrosion behaviour of electrodeposited and sputtered Cr coatings and sputtered Ta coatings with α and β phases

S. Maeng [a,*], L. Axe [a], T.A. Tyson [b], P. Cote [c]

[a] Department of Civil and Environmental Engineering, New Jersey Institute of Technology, Newark, NJ 07102, USA
[b] Department of Physics, New Jersey Institute of Technology, Newark, NJ 07102, USA
[c] U.S. Army Armament Research, Development and Engineering Center, Benet laboratories, Watervliet, NY 12189, USA

Received 2 December 2004; accepted in revised form 18 August 2005
Available online 14 October 2005

Abstract

The corrosion behaviour of α- and β-Ta coatings was compared to that of Cr coatings produced by cylindrical magnetron sputtering as well as electrodeposition. For Ta coatings, the corrosion process was dominated by dissolution of the steel substrate through open pores, however, at the end of 5 days, coating degradation was not observed. In contrast, while open pores were not observed with the Cr coatings, the corrosion resistance decreased as a function of time under acidic conditions, as a result of the protective oxide dissolution. Initially, however, the sputtered Cr coating exhibited improved corrosion resistance over the electrodeposited one, potentially due to the surface structure of the oxide film. Both Cr coatings showed similar transpassive behaviour to that of pure Cr; the current density of the sputtered Cr coating was observed to be greater than that of the electrodeposited one in the transpassive region due to the extensive droplet-like defects.

Keywords: Tantalum coating; Chromium coating; Magnetron sputtering; Electrochemical impedance spectroscopy; X-ray absorption spectroscopy; Corrosion behaviour

1. Introduction

Electrochemically deposited chromium coatings have been used as protective coatings against erosion and corrosion of gun bores because of their high wear and corrosion resistance [1,2]. However, hexavalent chromium is a known carcinogen and associated wastes are hazardous and difficult to dispose. Therefore, efforts have been made to replace electrodeposited (ED) Cr. They include physical vapor deposition (PVD) of Cr and a more environmentally friendly material and process such as magnetron sputtering of tantalum [2,3].

When deposited as a film on steel substrates, more than one phase of tantalum forms: α-phase (body centered cubic structure), which is stable and ductile, and β phase (tetragonal structure), which is meta-stable and brittle. Both α- and β-phases have been observed under varying PVD conditions [2,4,5]. Because of the brittle nature of the β-phase, α is preferred for the purpose of protecting gun bore against erosion. A metal coating without impurities or defects should exhibit corrosion behavior comparable to that of the bulk metal. However, in practice it is generally not feasible to achieve such coatings, especially for thin ones. Consequently, the potential presence of defects (i.e., pinhole, open pores) in coatings may result in severe localized corrosion [6]. Our previous study investigating the corrosion behavior of the α-Ta coating by planar magnetron sputtering showed that at 50 μm or greater, the coating behaves almost equivalently to the foil [7]. Furthermore, for thin Ta coatings (<10 μm), β-phase is more susceptible than α-phase to delamination due to localized corrosion at open pores.

The objective of this paper is to evaluate the corrosion behavior of PVD Ta and Cr coatings produced in full-scale processes and compare the performance to that of the ED Cr coating. Cylindrical magnetron sputtering was applied in producing α- and β-Ta coatings as well as Cr. Morphological

* Corresponding author. Tel.: +1 973 596 6077; fax: +1 973 596 5790.
E-mail address: smm8166@njit.edu (S. Maeng).

0257-8972/$ - see front matter © 2005 Elsevier B.V. All rights reserved.
doi:10.1016/j.surfcoat.2005.08.129

evaluation of the surface before and after electrochemical analysis was performed using scanning electron microscopy with energy dispersive X-ray spectroscopy for elemental analysis.

2. Experimental

The substrate for the Cr coatings is ASTM A723 (gun bore) steel cylinders. High contractile (HC) Cr with 100-μm thickness was electrochemically deposited; this is the conventional coating for gun bore [8]. The PVD Cr coating with 120 μm thickness was prepared by a cylindrical magnetron sputtering system. As for Ta coatings, the α-Ta with 38 μm and β-Ta with 50 μm were deposited on AISI 4340 steel also by a cylindrical magnetron sputtering.

In comparing coating performance, a number of analyses were conducted. To obtain local structural information of Cr and Ta coatings, extended X-ray absorption spectroscopy (EXAFS) experiments using total electron yield (TEY) mode were carried out at the Cr K edge (E_0=5989 eV) for Cr coatings and Ta L_{III} edge (E_0=9881 eV) for Ta coatings on beamline X11A at the National Synchrotron Light Source (NSLS), Brookhaven National Laboratory. The storage ring operated at the energy of 2.80 GeV with an average current of 180 mA. A Si (111) double-crystal monochromator was used for the photon energy selection, and the second Si crystal was detuned to approximately 50% (Cr coatings) and 80% (Ta coatings) of maximum transmitted X-ray intensity to minimize the presence of higher harmonics. EXAFS data were collected over the energy range of 5.839–7.093 keV for Cr coatings and a reference Cr foil and 9.732–10.986 keV for Ta coatings; spectra were analyzed following standard procedures [9]. Additionally, the crystallographic phase identification was accomplished using conventional X-ray diffraction (XRD) with Cu Kα radiation and the X-ray tube operating at 45 kV and 40 mA. Before and after corrosion tests, surface and corrosion features of coated samples were examined using an electron microscope with a field emission electron source and by energy dispersive X-ray spectroscopy (EDX) for elemental analysis. The corrosion products could therefore be qualitatively assessed at the pinhole defects.

In electrochemical investigations, solutions of deaerated 0.5 M H_2SO_4 were prepared with 10 N H_2SO_4 (ACS reagent grade) and deionized (DI) water. The systems were purged with N_2 gas

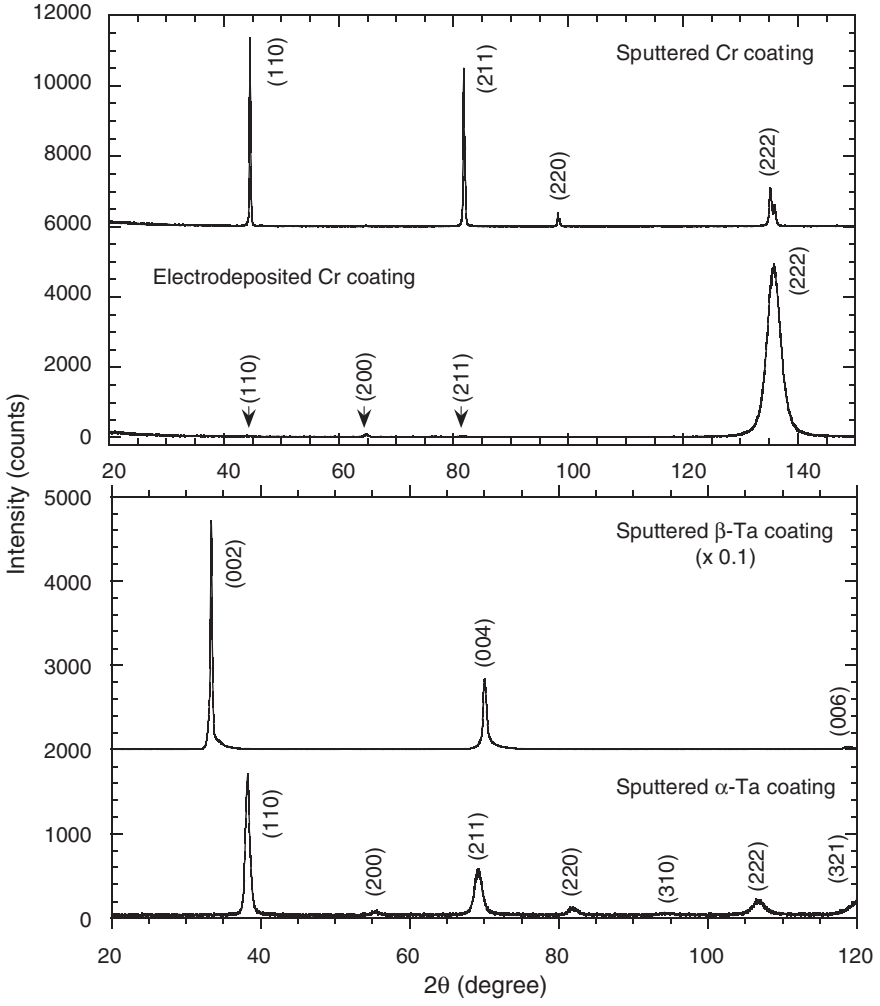

Fig. 1. X-ray diffraction patterns of electrodeposited Cr and sputtered Cr coatings and sputtered α- and β-Ta coatings.

(99.999% purity) at a rate of 1.0 L/min for 1 h before an electrochemical test and then continuously purged with the N_2 gas at a rate of 0.5 L/min during the experiment. Electrochemical impedance spectroscopy (EIS) and potentiodynamic polarization measurements were carried out at room temperature (22±3 °C) using a Gamry PC4/300 computerized system for collecting and analyzing electrochemical data. A flat cell (Princeton Applied Research) was used with a three-electrode configuration including a saturated calomel electrode (SCE) and platinum gauze as reference and auxiliary electrodes, respectively. All electrochemical tests were carried out with an exposure area of 1 cm^2.

EIS data were collected at open circuit potential (OCP) with a sinusoidal voltage perturbation of 10 mV (rms) over the frequency range of 10 mHz to 100 kHz with 7–10 points per decade; these spectra were obtained over an exposure period of 5 days. The data were analyzed using complex nonlinear least squares fitting (CNLS) LEVM algorithm [10] in the Gamry Echem Analyst software. Potentiodynamic polarization was measured 1 h after immersion with a scan rate of 10 mV/min from −0.2 to +1.5 V versus OCP.

3. Results and discussions

3.1. Phase identification and morphology

The ED and sputtered (PVD) Cr coatings reveal the same phase as the powder diffraction pattern of Cr (body centered cubic structure): the PVD Cr coating has (110) orientation and is similar to that of the Cr powder diffractogram, while the ED Cr coating has (222) orientation with peak broadening, which may be attributed to microstrain and particle size (Fig. 1). In addition

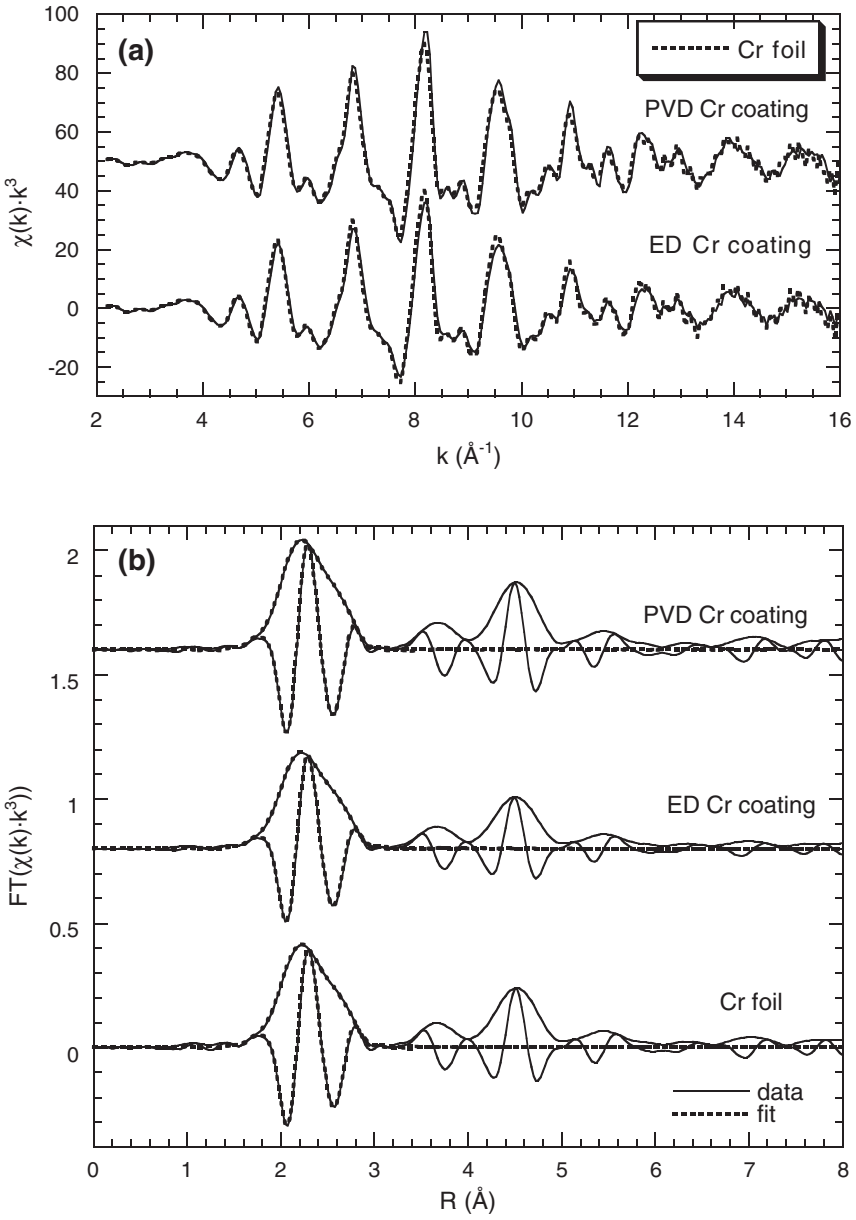

Fig. 2. (a) Cr *K*-edge $\chi(k)k^3$ spectra of PVD and ED Cr coatings and Cr foil. (b) Fits to Fourier transforms of $\chi(k)k^3$ spectra over the *k* range 2.4–15.7 $Å^{-1}$.

to the long-range structure, the short range structure of the Cr coatings was compared to that of the Cr foil by conducting EXAFS analysis. Data reduced to $\chi(k)k^3$ versus photoelectron wavevector, k, (Fig. 2a) show identical envelopes, where the PVD appears to exhibit less disorder due to the greater amplitude of the spectra compared to that for the ED coating. The Fourier transforms (FT) of the EXAFS ($\chi(k)k^3$) spectra (Fig. 2b) over 1.56–3.15 Å correspond to the first coordination shell that represents two subshells in the vicinity of the absorbing atom. This atomic short-range structure is consistent with Cr foil (body centered cubic structure) (Table 1) with 8 and 6 Cr atoms at 2.50 and 2.88 Å, respectively. It is interesting to note that the long-range order as well as the short-range structure is affected by deposition methods.

The α-Ta coating exhibits a very similar pattern to Ta powder with (110) orientation; the β phase was not observed (Fig. 1). For the β-Ta coating, three peaks (Fig. 1), referred to as (002), (004), and (006), are observed with no trace of the α phase. In general, β-Ta films exhibit (002) texture [11]. The short-range structure revealed unique structures (Fig. 3a). For the α-Ta coating, the FT of the $\chi(k)k^3$ over 1.7–3.05 Å corresponds the first coordination shell (Ta) around the absorbing atom (Fig. 3b); the atomic short-range structure is consistent with the theoretical EXAFS of α-Ta with 8–9 Ta atoms at 2.83 Å (Table 2). As for β-Ta coating, the broad shell of Ta is positioned between 1.7 and 3.5 Å. Given the β-Ta structure (tetragonal) with space group of $P\bar{4}2_1m$ and 30 atoms per unit cell [12], multiple subshells are present and therefore fitting was not feasible due to the number of parameters required in fitting exceeding the degrees of freedom. Jiang et al. [13] reported that as β-Ta has a highly disordered local structure, the EXAFS data can not be modeled by a simple cumulant expansion.

A morphological analysis of the ED Cr coating reveals a dense network of microcracks (Fig. 4a), which may be produced by internal stresses generated during electrodeposition [14]. Cote et al. [8] reported that the surface cracks were generated during deposition and subsequent annealing at 200 °C to remove hydrogen. These cracks are thin (<0.4 μm) as compared to the coating thickness (Fig. 4b); in addition, they are observed throughout the deposit. The PVD Cr coating does not exhibit microcracks, however, droplet-like defects (Fig. 4c) that are commonly found in PVD processes are seen throughout the surface; this feature has been reported by others as well [7,15–17]. SEM imaging of the α- and β-Ta coatings showed uniform coverage of the steel substrate without cracks (Fig. 5a and c). Nevertheless, defects such as droplet-like clusters and pinholes (Fig. 5b and d) were observed, but not to the same degree as that found with the PVD Cr coating (Fig. 4c). Defects in the form of open pores or voids extending from the coating surface to the substrate are of the greatest concern as they provide channels for electrolyte penetration to the steel substrate, initiating localized corrosion that significantly influences the corrosion resistance of coatings.

Table 1
Results of EXAFS fits[a] on the first shell for PVD and ED Cr coatings and Cr foil; Fourier transformed over 2.4–15.7 Å^{-} super 1 k-range and fitted over 1.56–3.15 Å r-range

	PVD Cr coating	ED Cr coating	Cr foil	Cr XRD model
First subshell (Cr–Cr)				
N[b]	8.0	8.0	8.0	8.0
R (Å)	2.50	2.50	2.50	2.49
σ^2 (Å^2)	0.003931± 2.9E-5	0.004796± 3.5E-5	0.004332± 4.4E-5	0
Second subshell (Cr–Cr)				
N[b]	6.0	6.0	6.0	6.0
R (Å)	2.88	2.88	2.88	2.88
σ^2 (Å^2)	0.003628± 5.3E-5	0.004482± 6.3E-5	0.004076± 1.12E-4	0

N, R, and σ^2 are coordination number, interatomic distance, and Debye-Waller factor, respectively.
N and R have error of ±20% and ±0.02 Å, respectively.
[a] S_0^2 was set as 0.74 based on fit on Cr foil.
[b] N was fixed in all fits.

3.2. Corrosion behaviour of as function of immersion time evaluated by EIS

The impedance spectra of the α- and β-Ta coatings collected over 4 days at OCP are shown in Fig. 6. Development of two time constants in the phase angle was observed for both coatings after 24 h of exposure. This effect was accompanied by a continuous and slight decrease in the absolute values of impedance. In general, tantalum exhibits consistent and stable impedance behaviour with one time constant over long exposure times due to the very stable and dense tantalum oxide passive film [18]. Therefore, the presence of two time constants is attributed to dissolution of steel substrate at open pores. The short relaxation time constant, associated with a high-frequency process is related to the coating/solution interface and the dielectric characteristic of the native oxide film, whereas the low-frequency process is associated with the substrate/solution interface through open pores.

For the Ta coatings, the equivalent circuit model (Fig. 7) applied in fitting the data represents localized corrosion of the steel substrate exposed to the electrolyte through permeable defects in the coating. The parallel connection of R_{ps} and C_s is representative of the electrical charge transfer process at the steel substrate/coating interface through open pores and represents the polarization resistance of the steel substrate and the capacitance of the electrical double layer at the electrolyte-steel substrate interface, respectively. R_{po} in series with R_{ps} and C_s is the pore resistance to the ionic current and provides information on degradation of the coating [19]:

$$R_{po} = \frac{\rho L}{PA} \tag{1}$$

where ρ is the resistivity of electrolyte in pores, L is average pore length and is equivalent to the coating thickness, A is the surface area exposed to electrolyte, and P is the porosity of the coating, that is the pore area per total exposed area. The circuit parameters obtained from EIS fitting are plotted as a function of

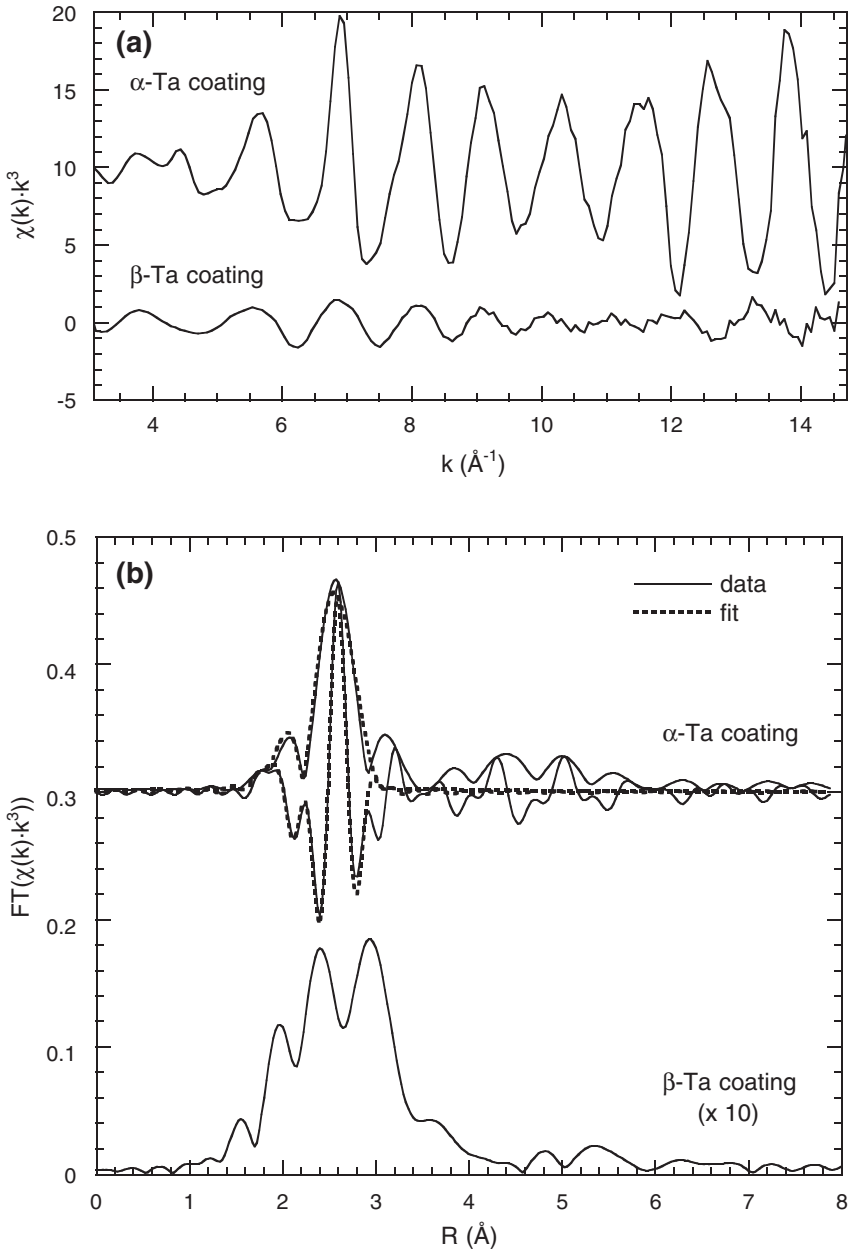

Fig. 3. (a) Ta L_{III}-edge $\chi(k)k^3$ spectra of PVD α- and β-Ta coatings. (b) Fourier transforms over the k range 3.1–15.4 $Å^{-1}$ for α-Ta coating and 3.5–14.1 $Å^{-1}$ for β-Ta coating.

time in Fig. 8. Both coatings show an increase in R_{po} at initial exposure; R_{po} of the α-Ta coating remains constant after 24 h, while for the β-Ta coating it shows a continuous increase. This increase in R_{po} appears to be due to blocking of pores, especially very fine ones from corrosion products along pore surfaces, decreasing porosity. Therefore, the β-Ta coating may have finer pores than the α-Ta coating. In contrast to R_{po}, both coatings exhibit a reduction in R_{ps}, suggesting dissolution of the steel substrate through open pores, yet the dissolution rate overall is not significant over the course of the experiment. The slight increase in R_{ps} for the β-Ta coating after 72 h of exposure may be due to the passivation of the steel substrate through open pores. In association with the behavior of R_{ps}, the increase in C_s demonstrates an increase in the corroding area at the steel substrate/coating interface. Using SEM, the surface morphology of both coatings was not observed to change over long exposure time and hence the coating capacitance (C_c) was

Table 2
Results of EXAFS fit[a] on the first shell for α-Ta coating on the steel substrate Fourier transformed over 2.85–15.8 $Å^{-1}$ k-range and fitted over 1.70–3.05 Å r-range

	α-Ta coating	α-Ta XRD model
N	8.97	8.00
R (Å)	2.83	2.86
σ^2 ($Å^2$)	0.006731±9.0E−5	0

N, R, and σ^2 are coordination number, interatomic distance, and Debye-Waller factor, respectively.

[a] S_0^2 was set as 1.0. N and R have error of ±20% and ±0.02 Å, respectively.

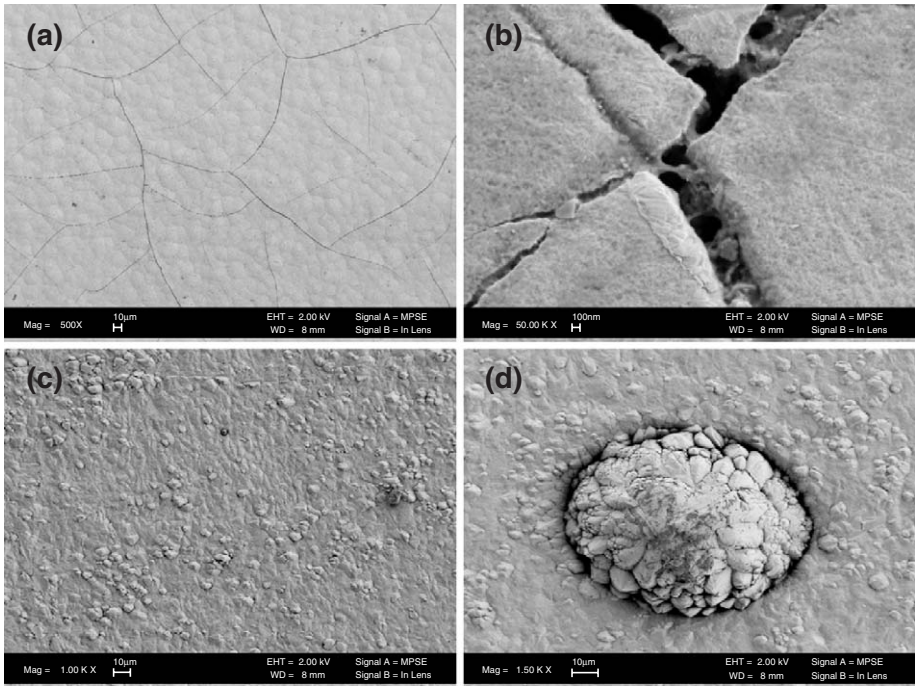

Fig. 4. SEM images of electrodeposited Cr (a, b) and sputtered Cr (c, d) coatings.

constant, indicating a lack of coating degradation. These results reveal that the corrosion process for Ta coatings is dominated by dissolution of the steel substrate through open pores. Therefore, the corrosion resistance of α- and β-Ta coated steels is highly dependent on the presence of open pores. In our earlier study [7], we found that for α-Ta coatings greater than 50 μm, a viable coating was produced where through-pores were insignificant; the impedance behavior was consistent with Ta foil. While the α-Ta coating evaluated in this current work is less than 50 μm, the β-Ta coating is approximately 50 μm. Interestingly, this thicker coating exhibited finer pores, however, the structure and properties are significantly different from the α phase, potentially contributing to the coating behaviour and localized corrosion.

The corrosion behaviour of the ED and PVD Cr coatings was also studied using EIS (Fig. 9). The impedance of the ED Cr coating decreases dramatically, reaching the lowest magnitude

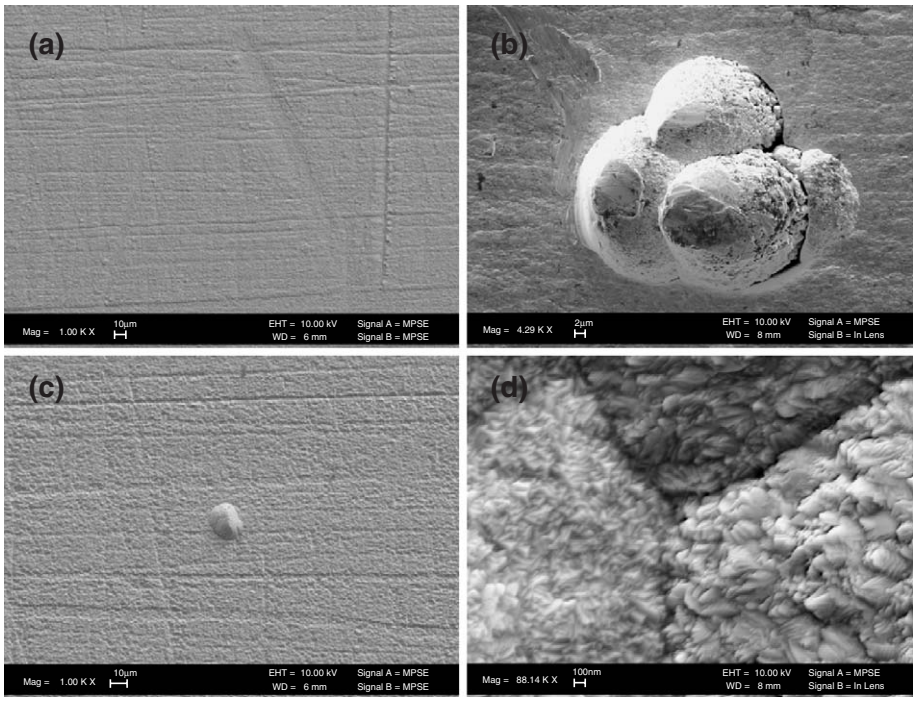

Fig. 5. SEM images of sputtered α-Ta (a, b) and β-Ta (c, d) coatings.

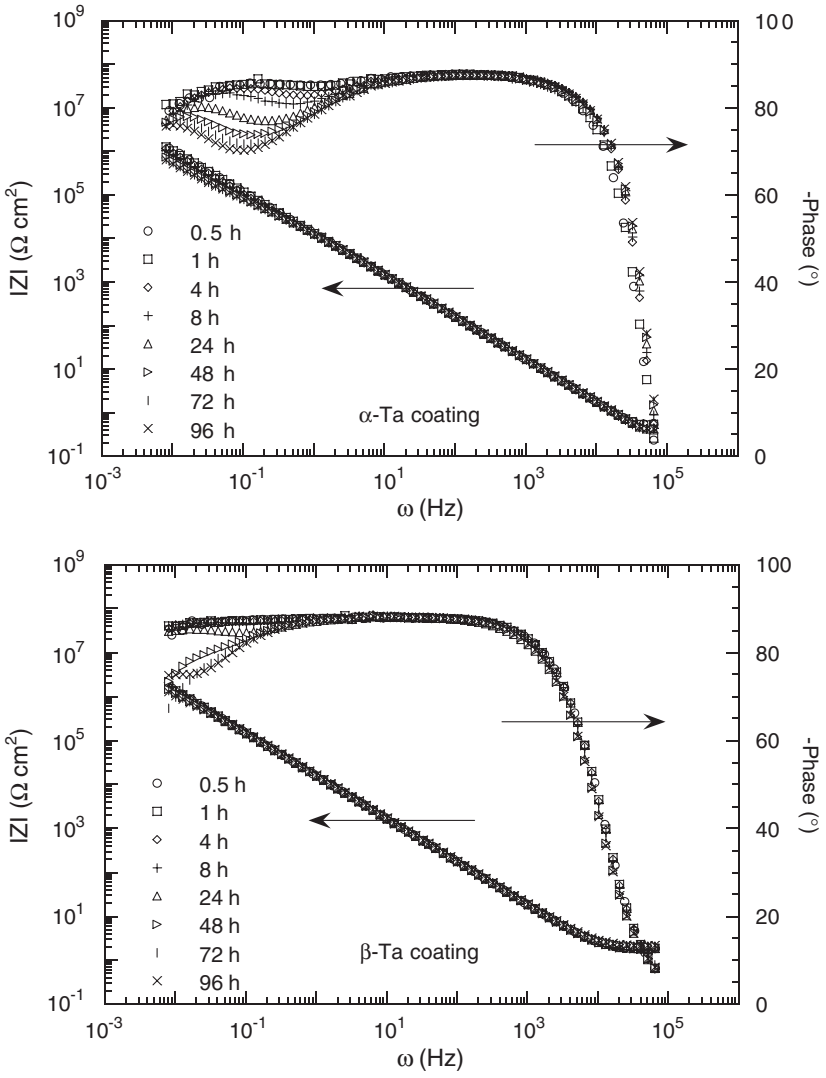

Fig. 6. Impedance spectra of sputtered α-Ta and β-Ta coatings for different immersion time in deaerated 0.5 M H_2SO_4 with N_2 at room temperature.

after 2 h exposure, whereas the PVD Cr coating shows only a relatively small decrease in the impedance, maintaining high impedance (over long exposure). In the initial phase angle response, two time constants were observed for both coatings. However, the ED Cr coating showed the transition to one time constant at 2 h, while two time constants were still seen for the PVD Cr up to 96 h of exposure. Cheng et al. [20] reported a transition in phase angle response from one time constant to two as potential increased from the active dissolution region to the passivation region for pure Cr. Therefore, the presence of two time constants in the Cr coatings may be attributed to the pre-existing passive film and/or any potential open pores as observed for the Ta coatings.

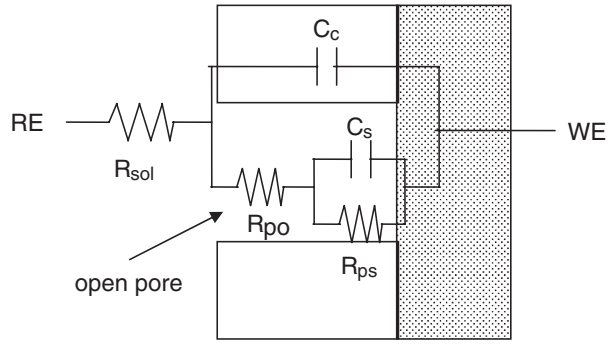

Fig. 7. Equivalent circuit model for fitting experimental EIS data of α-Ta and β-Ta coatings. (RE and WE are reference and working electrodes, respectively. R_{sol}: solution resistance, R_{po}: pore resistance, R_{ps}: polarization resistance of steel substrate, C_s: electrical double layer capacitance at steel/electrolyte interface, C_c: coating capacitance).

The passive film formed on Cr, reported as Cr_2O_3 [21], is not stable at pH less than 1 over the potential range of −1.2 to 2.2 V and hence, undergoes dissolution [22,23]. The OCP decayed with immersion time to more active values, resulting from dissolution. This decay was observed in both Cr coatings over the course of the experiment; for the ED Cr coating, from −438 to −732 mV (vs. SCE) at which the pure Cr foil corrosion potential was reported by Wilde and Hodge [23], and for the PVD Cr coating, from 75 to −290 mV (vs. SCE), where the pure Cr foil still undergoes passivation.

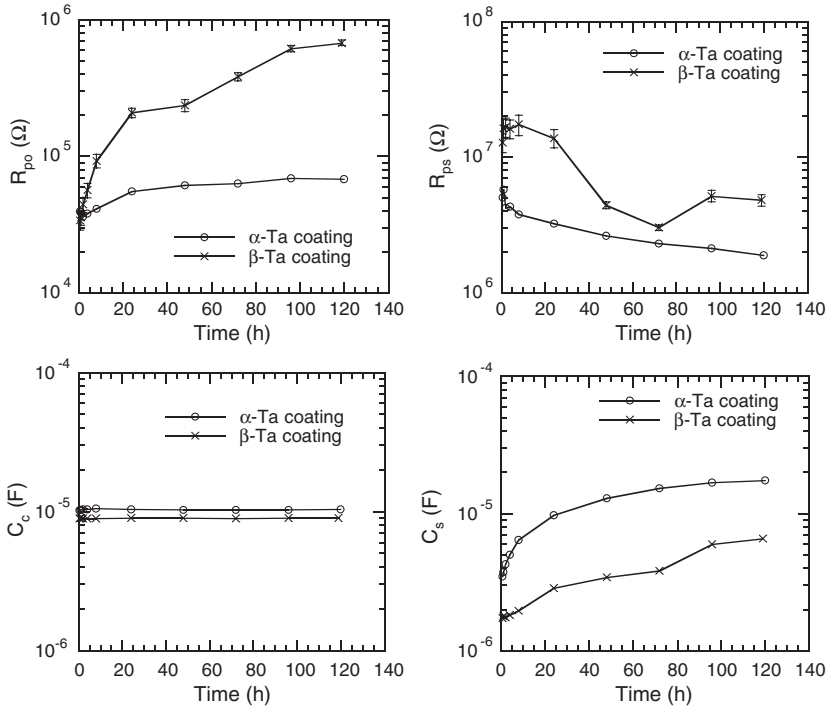

Fig. 8. The evolution of fitted parameters of the equivalent circuit for α-Ta and β-Ta coatings. Error bars not visible are present within symbol.

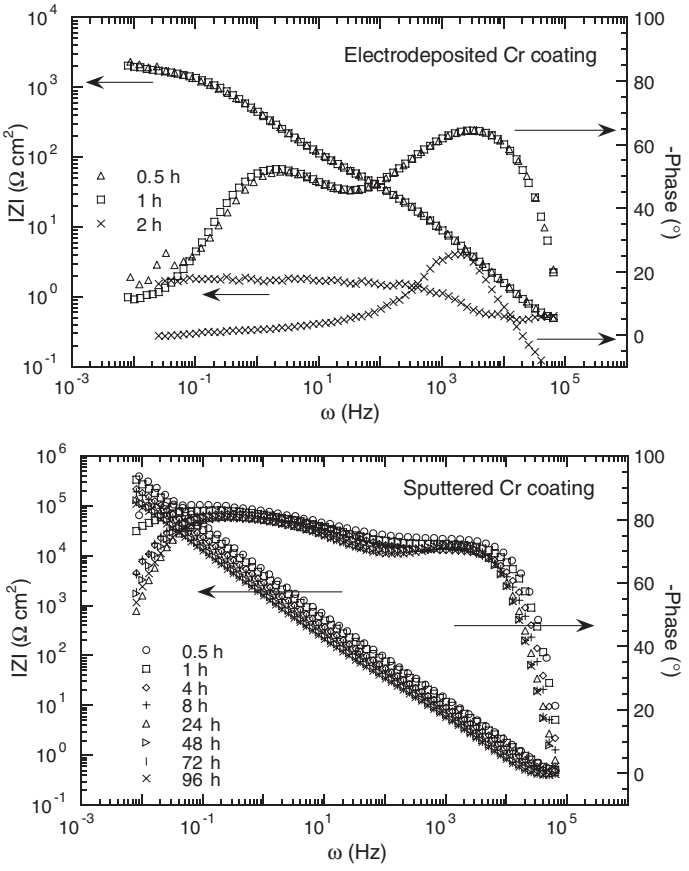

Fig. 9. Impedance spectra of electrodeposited Cr and sputtered Cr coatings for different immersion time in deaerated 0.5 M H_2SO_4 with N_2 at room temperature.

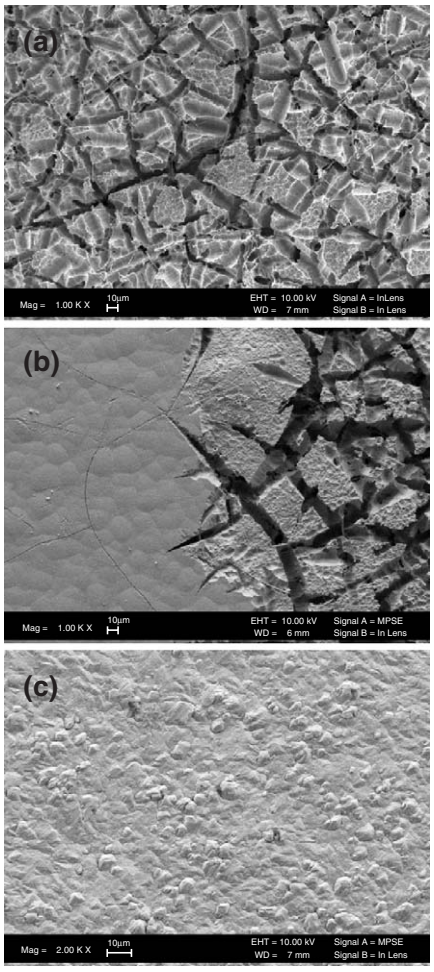

Fig. 10. SEM images of electrodeposited Cr (a, b) and sputtered Cr (c) coatings after EIS measurement.

Subsequent evaluation of the surface morphology of the ED Cr coating revealed severe attack, where dissolution was initiated at the microcracks (Fig. 10a and b). However, the PVD Cr coating does not show any effect of corrosion (Fig. 10c). Elemental analysis using EDX only confirmed the presence of Cr; yet, for coatings of such thickness, detecting the substrate even through μm size cracks would be very difficult (as EDX has a sampling depth of 1–2 μm). Therefore, potentiodynamic polarization was conducted to further assess the effect of open pores at 1 h after immersion by applying potential from −0.2 to 1.5 V (vs. SCE) from the OCP.

3.3. Anodic polarization behaviour of Cr coatings

The polarization curves for the ED and PVD Cr coatings are shown along with the steel substrate in Fig. 11. The behavior of the ED Cr coating is consistent with that of pure Cr foil in deaerated 0.5 M H_2SO_4 [23], showing two stable mixed potentials for the reduction of H^+ to H_2; its corrosion potential was measured at −660 mV (vs. SCE), which is slightly greater than that of pure Cr (−703 mV), indicating that the coating underwent active dissolution at the OCP. However, the PVD Cr coating, of which the corrosion potential was approximately −75 mV (vs. SCE), exhibits a more noble behaviour than the ED Cr coating. Additionally, the corrosion current density of the former is four orders of magnitude smaller than the latter. This result demonstrates that the PVD Cr coating is more corrosion resistant than that of the ED coating, potentially due to the passive oxide film.

Both Cr coatings show a similar transpassivation behaviour to that of pure Cr, representing oxidation of the passive film and dissolution of Cr species [24]. As the applied potential draws

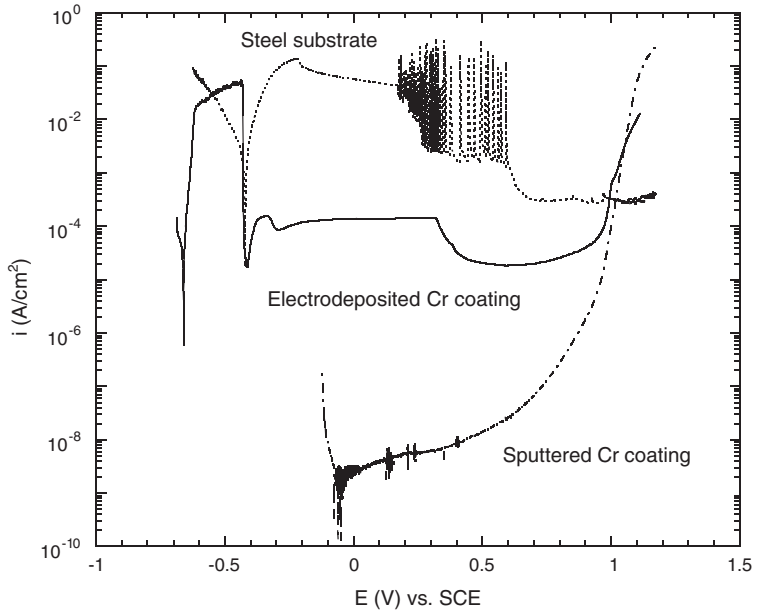

Fig. 11. Anodic polarization curves of electrodeposited Cr and sputtered Cr coatings and the steel substrate (ASTM A723) after 1 h immersion in 0.5 M H_2SO_4 deaerated with N_2 at room temperature.

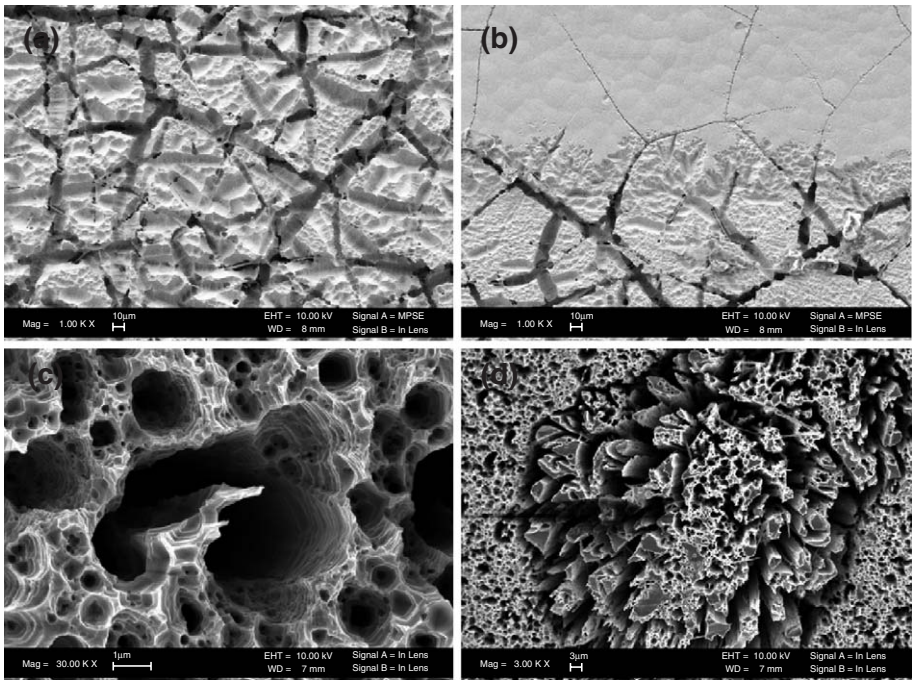

Fig. 12. SEM images of electrodeposited Cr (a, b) and sputtered Cr (c, d) coatings after potentiodynamic polarization measurement.

near the transpassivation region (>approx. 0.9 mV vs. SCE), the current density of the PVD Cr coating gradually increases, approaching that of the ED Cr coating. Interestingly, the current density of the PVD Cr coating becomes greater than that of the ED one beyond 1.05 V (vs. SCE). This result appears to be caused by the widespread droplet-like defects in the PVD Cr coatings, of which boundaries potentially provide more surface activity than that for the ED one. The surface morphology of the corroded ED Cr coating (Fig. 12a and b) is consistent with that observed at the free corrosion potential (Fig. 10a and b), showing microcracks are more severely attacked than other regions. In contrast, the PVD Cr coating exhibited a significant change in surface morphology; the surface became porous after dissolution of the Cr coating (Fig. 12c) and the droplet-like defects appear to be highly attacked (Fig. 12d). It is worth noting that at the transpassivation region of Cr coatings, the steel substrate is under passivation and hence corrosion products from substrate dissolution/oxidation at open pores may be observable by EDX for thinner Cr coatings ($\lesssim 3$ μm). However, substrate dissolution even in severely attacked regions was not confirmed. In association with EIS, these results potentially suggest a lack of open pores in the Cr coatings with thicknesses greater than 100 μm, indicating the corrosion process may be dominated by dissolution of the oxide film and oxidation of Cr species.

4. Conclusions

The corrosion behaviour of the PVD and ED coatings was studied at open circuit potential using EIS. For Ta coatings, the corrosion process was dominated by dissolution of the steel substrate through open pores, however, at the end of 5 days, coating degradation was not observed. In contrast, open pores were not observed with the ED and PVD Cr coatings. Yet a continuous decrease in the corrosion resistance was observed for the Cr coatings under acidic conditions, as a result of the protective oxide dissolution. In addition, the PVD Cr coating exhibited improved corrosion resistance over the ED one, which may be due to surface structure of the oxide film. Similarly, the polarization behaviour of the ED Cr coating was consistent with pure Cr, while the PVD one again showed improved corrosion performance. Both Cr coatings exhibited similar transpassive behaviour to that of pure Cr; the current density of the PVD Cr coating was observed to be greater than that of the ED one in the transpassive region, and again this may be attributed to the surface microstructure of the extensive droplet-like defects.

Acknowledgements

This work was conducted by NJIT as part of the Sustainable Green Manufacturing Program, through the National Defense Center for Environmental Excellence, contract DAAE30-98-C-1050.

References

[1] S.L. Lee, M. Cipollo, D. Windover, C. Rickard, Surf. Coat. Technol. 120–121 (1999) 44.
[2] S.L. Lee, D. Windover, M. Audino, D.W. Matson, E.D. McClanahan, Surf. Coat. Technol. 149 (2002) 62.
[3] D.W. Matson, E.D. McClanahan, S.L. Lee, D. Windover, Surf. Coat. Technol. 146–147 (2001) 344.
[4] L. Gladczuk, A. Patel, C. Singh Puar, M. Sosnowski, Thin Solid Films 467 (2004) 150.
[5] A. Jiang, T.A. Tyson, L. Axe, L. Gladczuk, M. Sosnowski, P. Cote, Thin Solid Films 479 (2005) 166.
[6] I.M. Notter, D.R. Gabe, Corros. Rev. 10 (1992) 217.

[7] S. Maeng, L. Axe, T.A. Tyson, L. Gladczuk, M. Sosnowski, Corros. Sci. (in press).
[8] P.J. Cote, G. Kendall, M.E. Todaro, Surf. Coat. Technol. 146–147 (2001) 65.
[9] B.K. Teo, Extended X-ray Absorption Spectroscopy: Basic Principles and Data Analysis, Springer-Verlag, New York, 1986, p. 114.
[10] J.R. Macdonald, Impedance Spectroscopy, John Wiley & Sons, New York, 1987, p. 173.
[11] M.H. Read, D.H. Hensler, Thin Solid Films 10 (1972) 123.
[12] A. Arakcheeva, G. Chapuis, V. Grinevitch, Acta Crystallogr., B 58 (2002) 1.
[13] A. Jiang, A. Yohannan, N.O. Nnolim, T.A. Tyson, L. Axe, S. Lee, P. Cote, Thin Solid Films 437 (2003) 116.
[14] L. Fedrizzi, S. Rossi, F. Bellei, F. Deflorian, Wear 253 (2002) 1173.
[15] C. Liu, Q. Bi, A. Leyland, A. Matthews, Corros. Sci. 45 (2003) 1257.
[16] S. Lee, W. Ho, F.D. Lai, Mater. Chem. Phys. 43 (1996) 266.
[17] S.H. Ahn, J.H. Lee, J.G. Kim, J.G. Han, Surf. Coat. Technol. 177–178 (2004) 638.
[18] O. Kerrec, D. Devillier, H. Groult, M. Chemla, Electrochim. Acta 40 (1995) 719.
[19] M. Kendig, F. Mansfeld, S. Tsai, Corros. Sci. 23 (1983) 317.
[20] X. Cheng, H. Ma, S. Chen, L. Niu, S. Lei, R. Yu, Z. Yao, Corros. Sci. 41 (1999) 773.
[21] M. Bojinov, G. Fabricius, T. Laitinen, T. Saario, G. Sundholm, Electrochim. Acta 44 (1998) 247.
[22] M. Pourbaix, Atlas of Electrochemical Equilibria in Aqueous Solutions, Pergamon Press, New York, 1966, p. 256.
[23] B.E. Wilde, F.G. Hodge, Electrochim. Acta 14 (1969) 619.
[24] S. Tanaka, N. Hara, K. Sugimoto, Mater. Sci. Eng., A Struct. Mater.: Prop. Microstruct. Process. 198 (1995) 63.